

# Space communications with variable elevation angle faded by rain: Radio links to the Sun–Earth first Lagrangian point $L_1$

Emilio Matricciani<sup>\*,†</sup>

*Dipartimento di Elettronica, Informazione e Bioingegneria, Politecnico di Milano, Piazza Leonardo da Vinci, 32  
20133 Milan, Italy*

## SUMMARY

How rain attenuation affects space links with variable elevation angles is not yet fully researched. The aim of this paper is to investigate this topic by simulating rain attenuation at  $K_a$  Band, in slant paths with variable elevation angles, with the Synthetic Storm Technique (SST), in links connected with spacecrafts at the Sun–Earth first Lagrangian point  $L_1$ , viewed from Spino d’Adda (Italy), Tampa (Florida), White Sands (New Mexico). The input to the SST is a large database of time series of 1-min rain rate recorded on site, 10 years in Spino d’Adda, 4 years at Tampa and White Sands. After recalling known results on the elevation angle of the Sun (i.e.  $L_1$ ),  $\theta_s$  ( $^\circ$ ), seen from latitude  $\lambda$  ( $^\circ$ ), I report what seems to be a new result: the mode of the probability density function of  $\theta_s$  in a year, in the range  $0 \leq \lambda \leq 90^\circ - \varepsilon$  (Earth axis tilt angle  $\varepsilon = 23.44^\circ$ ), coincides with the peak angle found at the day of the Winter solstice at the site, a result valid also for other planets, once their tilt angle is used. Compared to the complementary probability distribution function (pdf) of rain attenuation calculated for a geostationary (GEO) link (fixed elevation angle), the pdf to  $L_1$  depends on the rain-rate pdf during the contact time with  $L_1$ , according to the local climate. I show that, to obtain a good and easier estimate of the rain attenuation pdf in  $L_1$  links, we can consider a GEO link with elevation angle equal to the mean angle and rain rate pdf, both during the contact time, and that the mode angle gives an upper bound to the rain attenuation pdf in the sites considered. Copyright © 2015 John Wiley & Sons, Ltd.

Received 16 January 2015; Revised 26 June 2015; Accepted 9 July 2015

KEY WORDS: sun’s elevation angle; mean; mode; solstice; equinox; tropics; rain attenuation; Synthetic Storm Technique; Lagrange point  $L_1$ ;  $K_a$  band; Spino d’Adda; Tampa; White Sands

## 1. SLANT PATHS WITH VARIABLE ELEVATION ANGLES FADED BY RAIN

Differently from geostationary (GEO) satellites, all the other types of space orbits, including Low Earth Orbits (LEO), Medium Earth Orbits (MEO), High Elliptical Orbits (HEO) or orbits for interplanetary navigation, communicate with ground stations with radio links through slant paths in the troposphere with a time-variable elevation angle. The rate of change of this angle depends on the spacecraft orbit: it is the smallest for deep-space probes and the largest for LEO satellites. At frequencies greater than 10 GHz, all these radio links are faded by rain in a way that depends on carrier frequency, site weather, elevation angle and the impact of fade on system design and cost, according to the requirements on service unavailability (i.e. outage probability) in relation to the observation period (year, season and month) or mission duration.

How rain attenuation affects links with variable elevation angles is not yet fully researched, after the first pioneer works that reported statistics of rain attenuation in slant paths to the Sun obtained with sun trackers [1–7]. Today, the first and simplest approach is to predict rain-attenuation complementary probability distribution functions (pdf, for short) for fixed elevation angles, in discrete steps (sampling),

<sup>\*</sup>Correspondence to: Emilio Matricciani, Dipartimento di Elettronica, Informazione e Bioingegneria, Politecnico di Milano, Piazza Leonardo da Vinci, 32, 20133 Milan, Italy

<sup>†</sup>E-mail: Emilio.Matricciani@polimi.it

using one of the many prediction models that, from locally measured or estimated rain-rate pdf, calculates the rain-attenuation pdf at a desired frequency, and then to weigh the results according to the elevation-angle probability distribution function [8–11]. This method can give first reliable estimates if the observation period is 24 h, such as with a LEO satellite observed for long time.

In fact, a LEO satellite flies over a site many times in a day with different elevation angles, and therefore it is likely to sample, in a sufficiently long time, all possible rain events and elevation angles, day and night, above a minimum elevation angle required by system design for not suffering large tropospheric attenuation. This method, however, cannot be used for deep-space probes whose links are active only when the probe is viewed from the ground station (contact time) for part of the day, and for elevation angles greater than a minimum value. In other words, for deep-space spacecrafts we need conditional probability distribution functions of tropospheric attenuation, i.e. probability distribution functions of fades during the contact time.

In the following, we investigate this issue by studying, as an important example, radio links to a spacecraft located at the Sun–Earth First Lagrangian Point  $L_1$ , about 1.5 million km from Earth, around which the ESA/NASA Solar and Heliospheric Observatory (SOHO) is still orbiting.

We simulate rain-attenuation time series at 10, 19.7 and 32 GHz, in slant paths with time-variable elevation angle, by using a physical tool that, from locally measured rain-rate time series (rain events for short), can produce reliable rain-attenuation time series at a given frequency, elevation angle and polarization, namely the Synthetic Storm Technique (SST) [12].

We apply the SST to radio links to  $L_1$  viewed from sites with different meteorological conditions, namely Spino d’Adda (Italy), White Sands (New Mexico), Tampa (Florida) (Table I). The minimum elevation angle assumed depends in general on the frequency band. For instance, for deep-space communications, at 32 GHz ( $K_a$  Band) the NASA and the ESA require a minimum elevation angle in the range 10 to 20°. In the following I assume 20°. Obviously, only rain events during the contact time must be considered. Notice, however, that for space exploration missions, the current tolerated minimum availability during contact time is 0.99 (99%) (outage 0.01, 1% of the time), so that also the other components of the atmosphere (oxygen, water vapour and clouds) play a role in the link budget, although they are not considered in this paper. However, as always noticed in the history of technology, one limit today tends to be overcome tomorrow. Therefore, in my opinion, the required availability of deep-space communications will be pushed to approach that of satellite links, i.e. 0.001 (99.9%) and likely down to 0.0001 (99.99%) of the contact time; therefore, we need to know the rain attenuation pdf to this extent.

After this introductory text, Section 2 reports the relationship between solar time and clock (civil) time useful for calculating Sun elevation angle  $\theta_s$ , Section 3 summarises some results on  $\theta_s$ , as function of latitude. In this Section I also discuss what seems to be a new result: the mode (i.e. the most probable value) of the probability density function of  $\theta_s$  coincides with the peak angle found at the day of the Winter solstice, a result valid also for other planets. Section 4 discusses how to sample  $\theta_s(t)$  for rain attenuation calculations. Section 5 reports the most important statistical results on rain attenuation and shows that the rain-events data bank during the contact time with  $L_1$  can be statistically different from the long term one. Section 6 draws some conclusions. Appendix A lists mathematical symbols; Appendix B recalls the definition of the mode.

## 2. SOLAR TIME AND CLOCK TIME

To communicate with a spacecraft located at  $L_1$ , the ground station must follow its path in the sky during the daylight. But tracking  $L_1$  is just like tracking the Sun, with very little error in azimuth and

Table I. Sites considered in the simulation of rain attenuation with the Synthetic Storm Technique (SST) in variable-angle slant paths to  $L_1$ .

Site	Latitude (°N)	Longitude (°E)	Altitude asl (m)	Local mean horizontal wind (rain) speed (m/s)
Spino d’Adda (Italy)	45.40	9.50	84	10.6
Tampa (Florida)	27.60	277.70	15	8.3
White Sands (New Mexico)	32.54	253.39	1463	8.6

elevation angle, i.e. the angle to which rain attenuation is statistically sensitive. A simple exercise shows the order of magnitude of this error. Let us consider a site at 45° latitude, at the equinox, and let the Sun viewed at the local meridian (local solar noon). Standard plane geometry calculations yield that the elevation angle of the Sun is 44.998°, while that of L<sub>1</sub> is 44.827°, an error of the order of a tenth of degree, with no impact on rain attenuation. This means that we can assume the elevation angle of the Sun as if it were that of L<sub>1</sub>. Errors in azimuth are even less important.

Before calculating several interesting and new statistics of Sun's (i.e. L<sub>1</sub>) elevation angle, we must consider the relationship between the solar time and the clock time, also known as the civil time, recorded with the rain-rate time series, because at a site they can differ. If the time recorded with the rain-rate time series is the Universal Time, the formulae below can be applied once the civil time is restored.

When we transform a rain-rate time series into a rain-attenuation time series, the time axis of both is given by the local clock time,  $h_c$  (h) (no daylight saving time is applied in the following), regardless of the site longitude  $\phi$  (°E). In other words, the clock time may be the same for sites whose longitudes differ up to 15° (or more in special cases, which should be treated accordingly), while the solar time  $h_s$  (h) differs up to 1 h (or more). Because the Sun elevation angle,  $\theta_s$  (°), and consequently also the slant path elevation angle to L<sub>1</sub>, does depend on the solar time  $h_s$  (h), we have to calculate first  $h_s$  from  $h_c$ , before we can simulate rain attenuation times series for the smoothly and slowly changing elevation angle  $\theta_s(t)$  to L<sub>1</sub>.

The relationship between  $h_s$  and  $h_c$  is given by:

$$h_s = h_c + \frac{\tau}{60} + \frac{\phi - \phi_o}{15} \quad (h) \tag{1}$$

where  $\phi_o$  (°E) is the longitude of the next meridian to the East of the site, with longitude given by the first integer multiple of 15° (reference meridian,  $\phi_o > \phi$ );  $\tau$  (min) is a correction (the so-called Equation of Time [13]) given by:

$$\tau = 2.2918 \times [0.0075 + 0.1868 \times \cos B - 3.2077 \times \sin B - 1.4625 \times \cos(2B) - 4.089 \times \sin(2B)] \quad (\text{min}) \tag{2a}$$

with

$$B = (d - 1) \frac{2\pi}{365} \quad (\text{rad}) \tag{2b}$$

where  $d$  is the day number of the year. The parameter  $\tau$  (min), ranging from about -14 min to +16 min (see Figure 1), is necessary to correct the slowly changing speed of the Earth in its revolution around the Sun (because of Kepler's II law). For leap years 365 is substituted by 366.

An example illustrates the calculations. Let  $\phi = 253.39$  °E (White Sands),  $h_c = 12$  (noon),  $d = 1$ , then  $\tau = -2.9$  min,  $\phi_o = 255$  °E; therefore  $h_s = 12 - 2.9/60 + (253.39 - 255)/15 = 11.84$ , i.e. a negative difference of  $(12 - 11.84) \times 60 = 9.6$  min with the clock hour. Let  $\phi = 277.7$  ° (Tampa),  $d = 40$ ,  $\tau = -14.1$  min,  $\phi_o = 285$  °E, then  $h_s = 12 - 14.1/60 + (277.7 - 285)/15 = 11.28$ ; the difference is 43.2 min and thus there is a significant error between the clock time and the solar time, which would produce a wrong Sun elevation angle, because Tampa is West of the site (285°E) for which  $h_s = h_c = 12$ .

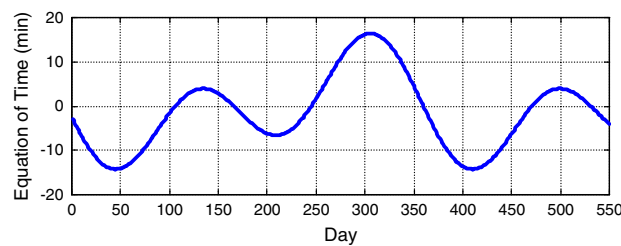


Figure 1. Equation of Time Notice that 365 + 185 days are drawn to show continuity.

### 3. SUN'S ELEVATION-ANGLE STATISTICS

The Sun elevation angle  $\theta_s$  ( $^\circ$ ) seen at a site at latitude  $\lambda$  ( $^\circ$ ) is given by:

$$\theta_s = \sin^{-1}(\cos \lambda \cos \delta \cos \omega + \sin \lambda \sin \delta) \quad (^\circ) \quad (3)$$

where  $\omega$  ( $^\circ$ ) is the angle between the meridian plane of the site and that of the Sun at the observation time  $h_s$ , given by:

$$\omega = 15 \times (12 - h_s) \quad (^\circ). \quad (4)$$

This latter parameter introduces time in (3) through (1).

In (3),  $\delta$  ( $^\circ$ ) is the Sun declination, given by Cooper equation [14]:

$$\delta = \varepsilon \times \sin\left(360 \times \frac{284 + d}{365}\right) \quad (^\circ). \quad (5)$$

In (5)  $\varepsilon = 23.44^\circ$  is the angle between Earth's rotational axis and the normal to the plane of its orbit around the Sun (tilt angle, obliquity);

Let us consider the Sun at the time it is seen at the longitude of the local meridian (local solar noon). Standard plane geometry calculations give the following relationships, as a function of latitude. They apply both to northern and southern hemispheres, if the latitude is taken as North or South.

The peak elevation angle at the day of the Summer solstice  $\Omega_{SS}$  ( $^\circ$ ) is given by:

$$\begin{aligned} \Omega_{SS} &= +\lambda + (90 - \varepsilon) & 0^\circ \leq \lambda \leq \varepsilon & \quad (^\circ). \\ \Omega_{SS} &= -\lambda + (90 + \varepsilon) & \varepsilon < \lambda \leq 90^\circ & \end{aligned} \quad (6)$$

In the range  $\varepsilon \leq \lambda \leq 90^\circ$ ,  $\Omega_{SS}$  is also the peak elevation angle of the year,  $\Omega_{MP}$  ( $^\circ$ ), for that latitude, while in the range  $0^\circ \leq \lambda \leq \varepsilon$ ,  $\Omega_{MP} = 90^\circ$ , as it can be calculated directly. In summary:

$$\begin{aligned} \Omega_{MP} &= 90^\circ & 0 \leq \lambda \leq \varepsilon \\ \Omega_{MP} &= \Omega_{SS} & \varepsilon < \lambda \leq 90^\circ. \end{aligned} \quad (7)$$

Figure 2 shows these relationships, together with others discussed below. The peak elevation angle at the day of the Equinox  $\Omega_E$  ( $^\circ$ ) is given (Figure 2) by:

$$\Omega_E = 90 - \lambda \quad 0^\circ \leq \lambda \leq 90^\circ \quad (^\circ). \quad (8)$$

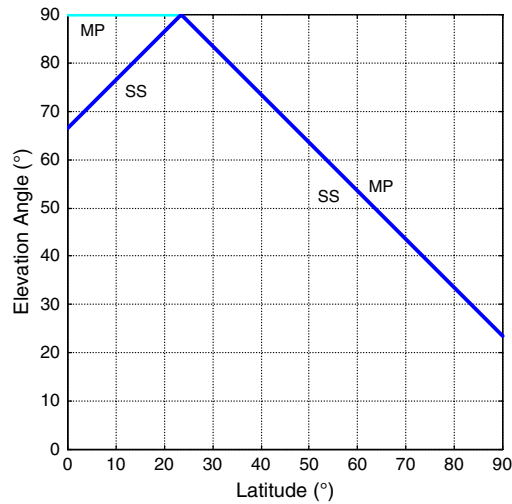
The peak elevation angle at the day of the Winter solstice,  $\Omega_{WS}$  ( $^\circ$ ), is given (see Figure 2) by:

$$\Omega_{WS} = -\lambda + (90 - \varepsilon) \quad 0^\circ \leq \lambda \leq 90^\circ - \varepsilon \quad (^\circ). \quad (9)$$

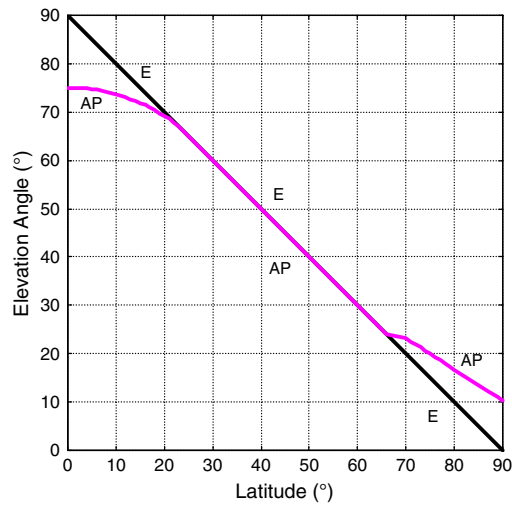
In the range  $0^\circ \leq \lambda \leq 90^\circ - \varepsilon$ , this is also the minimum peak elevation angle of the year, while for  $\lambda > 90^\circ - \varepsilon$  (latitudes northernmost the Arctic Circle), at the Winter solstice the Sun is below the horizon. In this range I have found (heuristically, see below) that the minimum peak of the year is  $\Omega_{mP} = +\lambda - (90 - \varepsilon)$ . In summary, the minimum peak elevation angle  $\Omega_{mP}$  ( $^\circ$ ) is given by:

$$\begin{aligned} \Omega_{mP} &= \Omega_{WS} & 0^\circ \leq \lambda \leq 90^\circ - \varepsilon & \quad (^\circ). \\ \Omega_{mP} &= +\lambda - (90 - \varepsilon) & \lambda > 90^\circ - \varepsilon & \end{aligned} \quad (10)$$

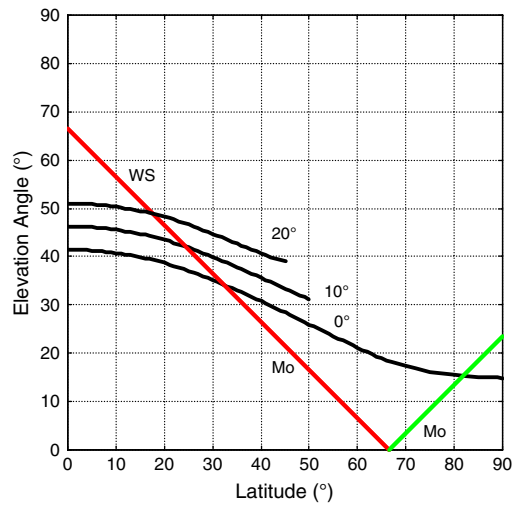
As an example, Figure 3 shows the elevation-angle time series at White Sands at the two solstices and (spring) equinox. Figure 4 shows the probability density function of the elevation angle of these three days. From Figures 4 and 3, we can notice, heuristically, an interesting property, namely that the most probable elevation angle of the day, i.e. the mode of the probability density function of the



(a)



(b)



(c)

Figure 2. Sun’s elevation peak angle as function of latitude: (a) Summer solstice  $\Omega_{SS}$  (SS, blue), maximum peak  $\Omega_{MP}$  (MP, cyan–blue); (b) Equinox  $\Omega_E$  (E, black–magenta), average peak  $\Omega_{dPm}$  (AP, magenta); (c) Winter solstice  $\Omega_{WS}$  (WS, red), mode  $\theta_\mu$  (Mo, red–green), also equal to the minimum peak  $\Omega_{mP}$ .

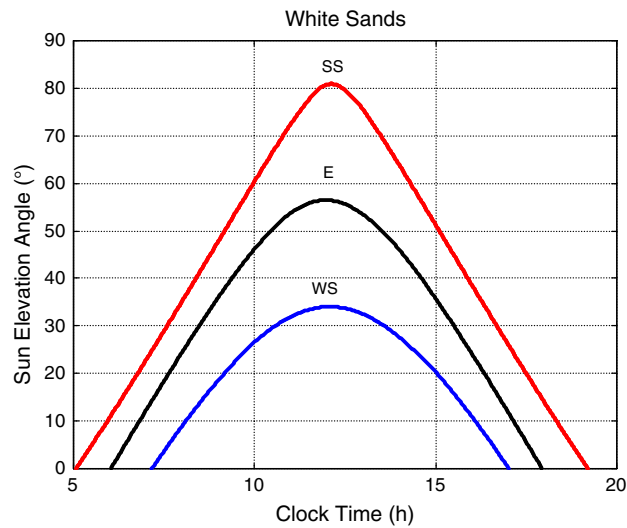


Figure 3. Elevation-angle time series at the two solstices (WS: Winter; SS: Summer) and Spring equinox (E), White Sands ( $\lambda = 32.54^\circ\text{N}$ ). Notice that the time scale is the clock (civil) time, not the solar time (the two differ according to (1)).

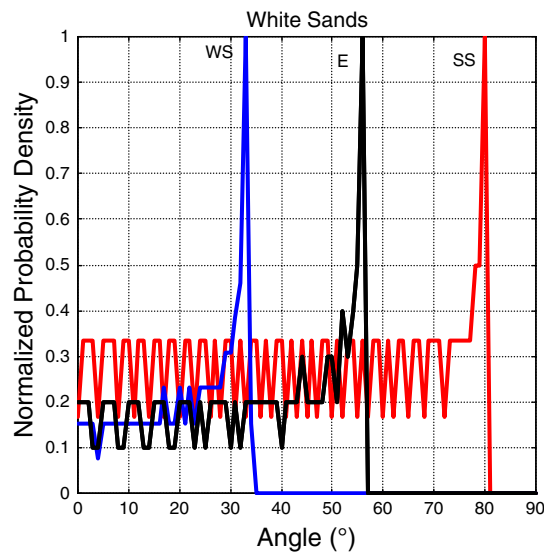


Figure 4. Normalized probability density function of the elevation angle of the Sun ( $L_1$ ), White Sands ( $\lambda = 32.54^\circ\text{N}$ ), at the Summer solstice (SS), Winter solstice (WS) and the equinox (E). For the purpose of clearly comparing the peaks, the densities are normalized to their peak (mode); therefore their integrals differ from one.

day (the peak in Figure 4),  $\theta_\mu$  ( $^\circ$ ), always coincides with the peak angle of that day (Figure 3). That the two angles coincide can be deduced from the time series shown in Figure 3: near the peak the rate of change of the Sun’s elevation angle decreases down to zero, therefore  $\theta_s(t)$  spends more time in an amplitude band  $\Delta\theta_s$  around the peak than around any other value in the same band. Figure 5 shows how the daily peak,  $\Omega_{dP}$  ( $^\circ$ ), changes in a year and also the time the Sun spends in an amplitude band  $\Delta\theta_s = 0.5^\circ$  just below the peak. In conclusion, in any day of the year the mode (i.e. the most probable value) and the peak coincide; therefore the mode is determined by the Sun–Earth orbit.

Moreover, a study of the statistics of the daily peak shown in Figure 5, each peak weighted identically (1 sample per day), shows, heuristically, that the mean value of  $\Omega_{dP}$ ,  $\Omega_{dPm}$  ( $^\circ$ ), always coincides in the range  $\varepsilon \leq \lambda \leq 90 - \varepsilon$  (Tropic of Cancer to the Arctic Circle, or Tropic of Capricorn to the Antarctic Circle)

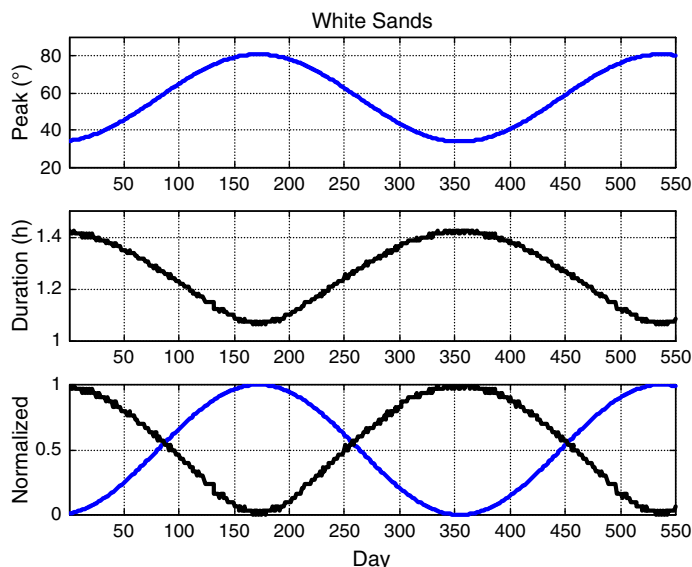


Figure 5. White Sands ( $\lambda = 32.54^\circ\text{N}$ ). Upper figure: Sun elevation peak  $\Omega_{MP}$  ( $^\circ$ ) (local solar noon) in a day of the year. Middle figure: Duration (h) spent by the Sun ( $L_1$ ) in a band of  $0.5^\circ$  below the peak at local solar noon. Lower figure: Curves normalized to the peak to compare the quasi-sinusoidal trends and anticorrelation. Notice that  $365 + 185$  days are drawn to show continuity. The minimum duration corresponds to the Summer solstice, the maximum duration to the Winter solstice. Vice versa for the peak angle.

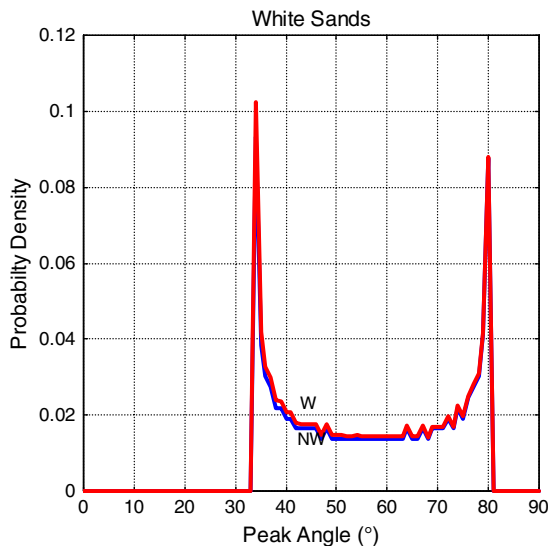


Figure 6. Probability density function of the daily peak, White Sands ( $\lambda = 32.54^\circ\text{N}$ ), weighted according to the duration shown in Figure 5 (red line, W), or with unitary weight (blue line, NW).

with the peak angle  $\Omega_E$  found at the equinox (Figure 2). Figure 6 shows the probability density function of the daily peak, at White Sands, weighted according to the duration spent by the Sun ( $L_1$ ) in a band of  $0.5^\circ$  shown in Figure 5, or with unitary weight. We notice that the two densities practically coincide, likely because the duration in Figure 5 is not too different from unity (1 h). The mean value of the distribution of unitary-weighted samples is  $57.46^\circ$  (e.g. from (7)), while the mean value of the weighted samples is  $55.89^\circ$ . Finally, Figure 2 shows the complete relationship  $\Omega_{dP}(\lambda)$  in the range  $0^\circ \leq \lambda \leq 90^\circ$ .

The mode found at the day of Winter solstice has, however, a wider meaning, as I show next.

Let us study the probability density function of  $\theta_s$  in a year, conditioned to the minimum elevation angle of observation. As an example, Figure 7 shows the density functions found at White Sands for different minimum elevation angle  $\theta_{\min}=0^\circ, 5^\circ, 10^\circ, 20^\circ$ . It clearly shows that the mode is a function only of the latitude. Therefore, in general, Figure 8 shows how the density function varies with latitude for  $\theta_{\min}=0^\circ$ .

A detailed study of the relationship between mode and latitude (as in Figure 8) is, at first sight, a little surprising. In fact, I have found that in the range  $0^\circ \leq \lambda \leq 90^\circ - \varepsilon$ , the mode coincides with the peak found at the same latitude at the Winter solstice,  $\Omega_{WS}$ , thus confirming the link to the Sun–planet orbit. This coincidence is likely because of the fact, already observed, that in any day of the year the mode and the peak coincide. Now, heuristically, when all data of the year are considered in a single probability density function, we can observe (see Figure 3) that in every day of the year any two symmetrical elevation angles below the Winter solstice peak are always sampled, while all other symmetrical angles around the peak of a day occur less frequently, as we approach the summer solstice, and that the longer

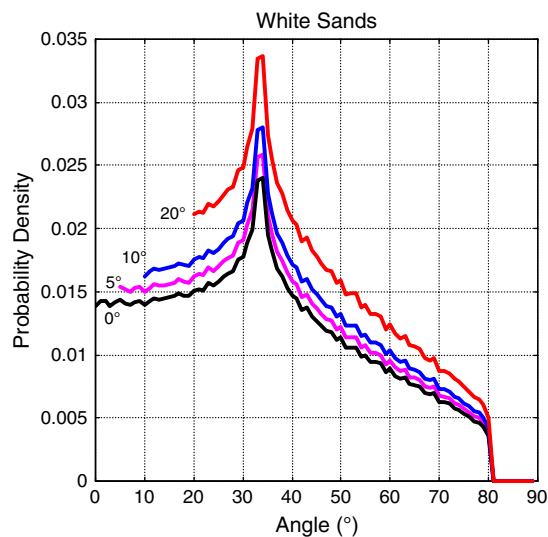


Figure 7. Probability density function of the elevation angle of the Sun ( $L_1$ ), White Sands ( $\lambda = 32.54^\circ \text{N}$ ), in a year, for different minimum elevation angles ( $0^\circ$ , black;  $5^\circ$ , magenta;  $10^\circ$ , blue;  $20^\circ$ , red).

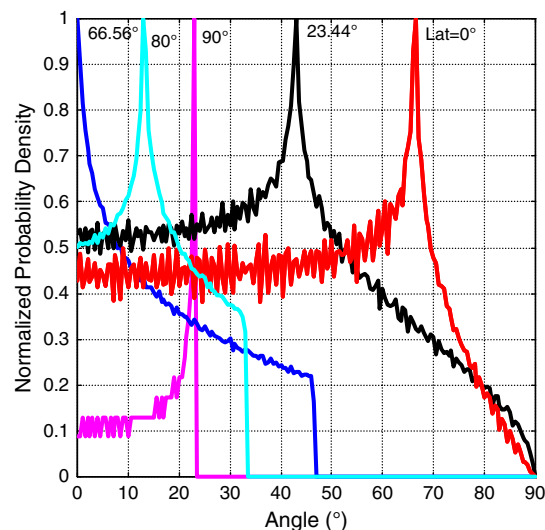


Figure 8. Probability density function of the elevation angle of the Sun ( $L_1$ ) at latitude  $\lambda=0^\circ$  (red),  $\lambda=\varepsilon$  (black),  $\lambda=90^\circ - \varepsilon$  (blue),  $\lambda=80^\circ$  (cyan),  $\lambda=90^\circ$  (magenta), in a year. All peak values can be calculated from (7) or Table II.

interval (amplitude band  $\Delta\theta_s$ ) always occurs at the Winter solstice. Besides this heuristic argument I could not find a mathematical proof in the literature (see Appendix B).

Finally, in the range  $90^\circ - \varepsilon < \lambda \leq 90^\circ$ , again heuristically, I have found that the mode increases linearly from  $0^\circ$  to  $\varepsilon$ . Therefore the overall relationship between the mode  $\theta_\mu(\lambda)$  and the latitude  $\lambda$  is given by:

$$\begin{aligned} \theta_\mu &= \Omega_{WS} & 0 \leq \lambda \leq 90^\circ - \varepsilon \quad (^\circ). \\ \theta_\mu &= \lambda - (90 - \varepsilon) & 90^\circ - \varepsilon < \lambda \leq 90^\circ \end{aligned} \tag{11}$$

In other words, up to the Arctic Circle (Antarctic Circle), the peak elevation angle observed at the Winter solstice at a site gives the most probable elevation angle of the Sun in all year, while northernmost (southernmost) the mode increases linearly from  $0^\circ$  to  $\varepsilon$ . Figure 2 shows also this relationship. We can extend this theorem by stating that, in any continuous period of the year, the mode of the Sun's elevation angle is given by the minimum daily peak angle of that period. Table II summarizes these relationships.

A similar study conducted on the mean elevation angle,  $\theta_m$  ( $^\circ$ ), as a function of the latitude, derived now with a best fit (hence an approximate relationship), gives (see the black line for  $\theta_{\min} = 0^\circ$ , Figure 2) the following relationship:

$$\theta_m = 13.29 \cos(2\lambda) + 28.17 \quad 0 \leq \lambda \leq 90^\circ \quad (^\circ). \tag{12a}$$

The dependence of  $\theta_m$  on  $\theta_{\min}$  can be found in the results shown in Figure 9, up to  $\theta_{\min} = 30^\circ$ ,

Table II. Sun's ( $L_1$ ) elevation-angle  $\theta_s$  ( $^\circ$ ) as a function of latitude  $\lambda$  ( $^\circ$ ). The relationships are valid both for the Northern and Southern hemispheres, if the latitude refers to one of the two. Notice that  $\lambda = \varepsilon$  is the latitude of the Tropic Circles,  $\lambda = 90^\circ - \varepsilon$  of the Arctic and Antarctic Circles.

Parameter	$0^\circ \leq \lambda \leq \varepsilon$	$\varepsilon < \lambda \leq 90^\circ - \varepsilon$	$90 - \varepsilon \leq \lambda \leq 90^\circ$
Summer Solstice Peak	$\Omega_{SS} = +\lambda + (90 - \varepsilon)$	$\Omega_{SS} = -\lambda + (90 + \varepsilon)$	$\Omega_{SS} = -\lambda + (90 + \varepsilon)$
Equinox Peak	$\Omega_E = -\lambda + 90$	$\Omega_E = -\lambda + 90$	$\Omega_E = -\lambda + 90$
Winter Solstice Peak	$\Omega_{WS} = -\lambda + (90 - \varepsilon)$	$\Omega_{WS} = -\lambda + (90 - \varepsilon)$	—
Maximum Peak	$\Omega_{MP} = 90^\circ$	$\Omega_{MP} = \Omega_{SS}$	$\Omega_{MP} = \Omega_{SS}$
Mean Peak (not weighted)	See Figure 2	$\Omega_{dPm} = \Omega_E$	See Figure 2
Minimum Peak	$\Omega_{mP} = \Omega_{WS}$	$\Omega_{mP} = \Omega_{WS}$	$\Omega_{mP} = +\lambda - (90 - \varepsilon)$
Mode	$\theta_\mu = \Omega_{WS}$	$\theta_\mu = \Omega_{WS}$	$\theta_\mu = +\lambda - (90 - \varepsilon)$

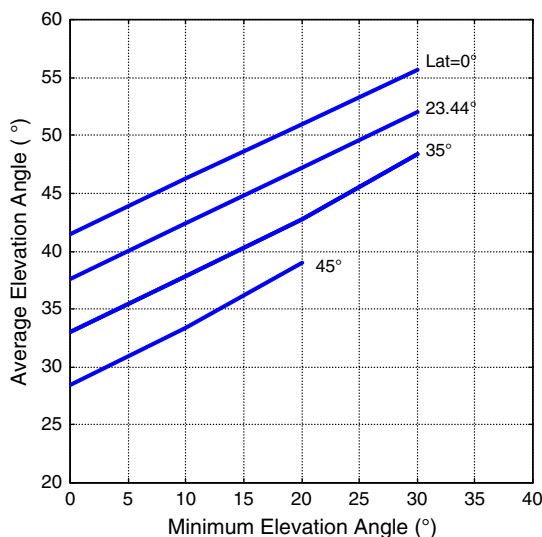


Figure 9. Average (mean) elevation angle of the Sun,  $\theta_m$  ( $^\circ$ ), as a function of the minimum elevation angle considered,  $\theta_{\min}$  ( $^\circ$ ). The slope of  $\theta_m$  is approximately  $5^\circ/\text{decade}$ .

obtained from the curves shown in Figure 8. As we can notice, the mean value increases approximately  $5^\circ/\text{decade}$  of  $\theta_{\min}$ , so that we can write (12a) as:

$$\theta_m = 13.29 \cos(2\lambda) + 28.17 + 0.5 \theta_{\min} \quad \theta_m \leq \Omega_{MP}, \theta_{\min} < 30^\circ \text{ (}^\circ\text{)}. \quad (12b)$$

From Figure 2 we can directly establish if the probability density function of  $\theta_s$ , at a given latitude, is skewed to the right ( $\theta_m > \theta_\mu$ ), or to the left ( $\theta_m < \theta_\mu$ ), for a given  $\theta_{\min}$ . The median value (value exceeded with probability 0.5) is always between the mode and the mean.

#### 4. ELEVATION ANGLE SAMPLING AND RAIN ATTENUATION CALCULATION

The input rain-rate data to the SST are rain-rate time series with rain-rate raw data (tips) averaged in 1-min intervals, recorded with conventional tipping-bucket rain gauges located at Tampa and White Sands, kindly made available to us by Roberto Acosta, formerly with NASA Glenn Research Center, and our own data bank of Spino d'Adda. A distinctive rain event (i.e. a rain-rate time series) is defined whenever the interval between two successive rain gauge tips is longer than 1 hour. The  $0^\circ\text{C}$  rain height adopted in these simulations is the ITU-R model [15]. A melting layer is modelled with melting hydrometeors at  $0^\circ\text{C}$ , falling vertically 400 m from the  $0^\circ\text{C}$  ITU-R rain height. The 400-m depth is the original melting layer model discussed in [16] and adopted in the SST [12], long time before the ITU-R adopted 360 m.

The parameters  $k$  and  $\alpha$  that give the specific rain attenuation  $kR^\alpha$  (dB/km) from the rain rate  $R$  (mm/h), integrated by the SST along the rainy path, depend, in general, on many variables such as frequency,

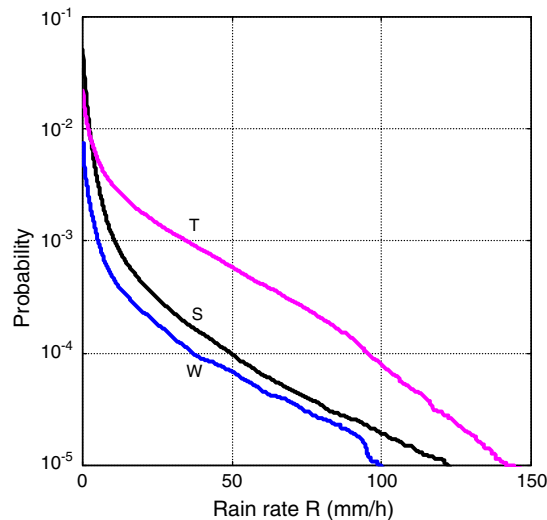


Figure 10. Rain-rate complementary probability distribution (pdf, or fraction of the observation time), in an average year, of Tampa (T, magenta), Spino d'Adda (S, black), White Sands (W, blue).

Table III. Rain rate data base, observation time and rainy time for  $\theta_s(t) \geq 20^\circ$  and, in parentheses, for  $\theta_s(t) \geq 10^\circ$ .

Site	Rain observation time (years)	Number of rain events	Number of rain events in $L_1$ contact time	$L_1$ contact time in a year (h)	Rainy time in a average year (h)	Rainy time in an average year in $L_1$ contact time (h)
Spino d'Adda	10.00	1412	403 (541)	2695.0 (3570.1)	449.9	117.6
Tampa	4.00	574	152 (191)	3167.6 (3760.4)	194.7	57.3
White Sands	4.42	255	52 (71)	3090.7 (3726.3)	66.1	16.1

polarization, elevation angle, drop-size distribution, water temperature, time. For long-term studies and predictions, we adopt values of  $k$  and  $\alpha$  that depend only on polarization (assumed circular in this paper) and temperature, once a drop-size distribution is assumed, such as those reported in [17] at 0 °C and 20 °C, useful for modelling the melting layer and the rain layer [12, 16]. We have adopted these constants, both in this work and in the previous studies with the SST because they provide a consistent and reliable set of data at 0 °C and 20 °C water temperatures.

Figure 10 shows the rain-rate complementary probability distribution functions exceeded in an average year. These are the unconditional input pdf to all prediction methods that predict rain-attenuation pdf for long-term continuous observation time (e.g. for Earth orbits), not for a spacecraft contact time, which needs conditional statistics. We show them because large differences can be noted in the rain rate of the sites, and also because they are used by the SST at zenith paths. Other important differences, such as the number of rainstorms and the rainy time in an average year, are reported in Table III.

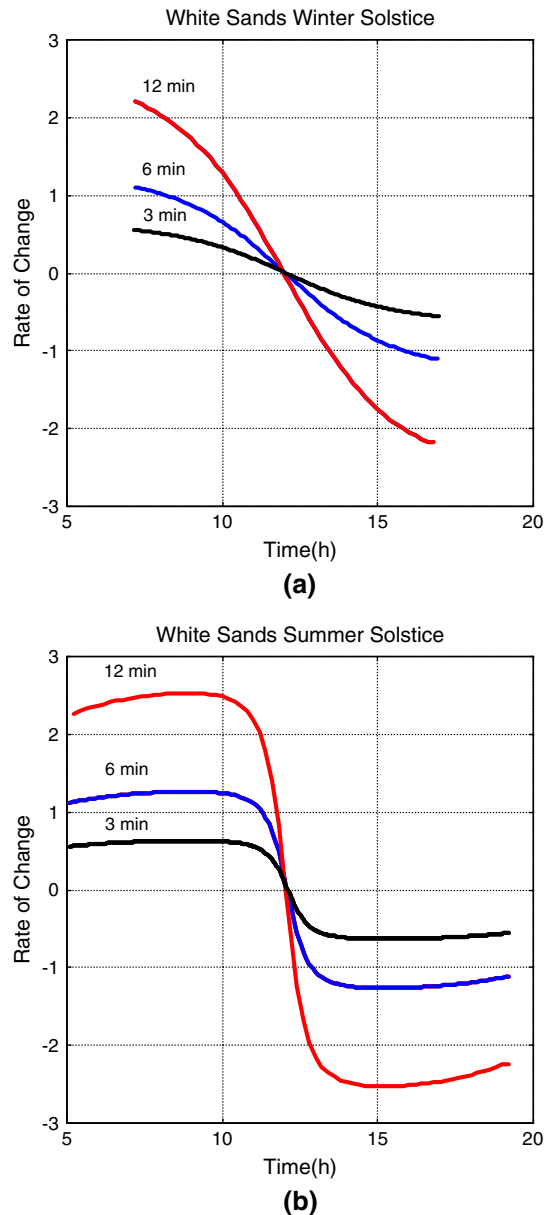


Figure 11. Rate of change of Sun’s elevation angle in the indicated intervals at White Sands: (a) at the Winter Solstice; (b) at the Summer solstice. Local clock time.

The SST was developed for calculating rain-attenuation time series in terrestrial or fixed slant paths, i.e. paths with constant elevation angle [12]. To estimate rain attenuation in a link to  $L_1$ , we have to apply the SST to a path with changing elevation angle. To achieve this goal, first we need to sample the Sun elevation angle  $\theta_s(t) \geq \theta_{\min}$ , and keep it constant for an interval of time in which the elevation angle does not change too much for rain attenuation calculations (tenths of dB). Notice that by using (3) we neglect the effects of the atmosphere because rain attenuation is insensitive to small changes of the angle of arrival of the electromagnetic wave (i.e. ray bending and defocusing).

In other words, for each interval of sampling time and corresponding elevation angle found at the beginning of the interval, the SST transforms the complete rain-rate time series of the event occurring at that time into a rain-attenuation time series calculated with that elevation angle (the elevation angle affects the speed of rainstorm along the slant path, which becomes infinite at zenith, see [12]). The complete rain-attenuation time series, i.e. the one that simulates the rain-attenuation time series that would be measured in the path with a continuously changing elevation angle  $\theta_s(t) \geq \theta_{\min}$ , is then obtained by adding all the non-overlapping (disjoint) pieces of rain-attenuation time series found in each interval, therefore obtaining a continuous rain-attenuation time series whose elevation angle changes in small steps, within the contact time of the day.

I have assessed empirically the length of such a fixed interval by studying the sensitivity of the long term rain-attenuation pdf to the interval length, and have found that 6 min is a good compromise, in any day of the year, between the need to describe rain attenuation with sufficient accuracy and the need to process a manageable number of rain-attenuation time series at constant elevation angle for each rain-rate time series.

For example, Figure 11 shows the rate of change of the Sun's elevation angle at the Winter solstice and in the Summer solstice in the indicated intervals (3, 6 and 12 min) at White Sands. We can see that in 6 min the change in elevation angle is well below  $2^\circ$ , a change that is negligible in the calculation of rain attenuation, as Figure 12 clearly shows.

The elevation angle is therefore sampled every 6 min, in small steps, according to the time of the day and to the day of the year and for each contiguous 6-min interval the SST is applied as if the elevation angle were constant. Figures 13 and 14 show some examples of the rain-attenuation time series obtained at 32 GHz at White Sands: (a) for the variable elevation angle to  $L_1$ , (b) for the minimum ( $20^\circ$ ) and (c) for the maximum ( $81^\circ$ ) values, kept fixed as if the links were to a GEO satellite, together with  $\theta_s(t)$ . We notice that the rain-attenuation time series for  $L_1$  is smooth, no

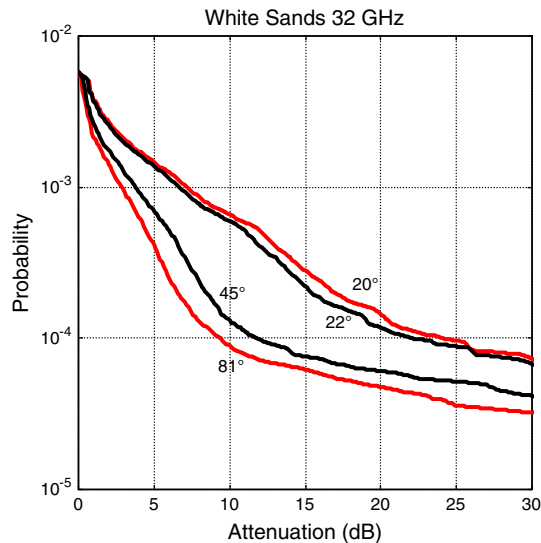


Figure 12. Complementary probability distribution functions (or fraction of the observation time) at 32 GHz, White Sands of a GEO satellite link, with an elevation angle  $\theta = 20^\circ$  (red line),  $22^\circ$  (black),  $45^\circ$  (black),  $81^\circ$  (red). At equal probabilities, a change of  $2^\circ$  yields a very small change in rain attenuation at the lowest elevation angles, and a negligible change at the largest ones.

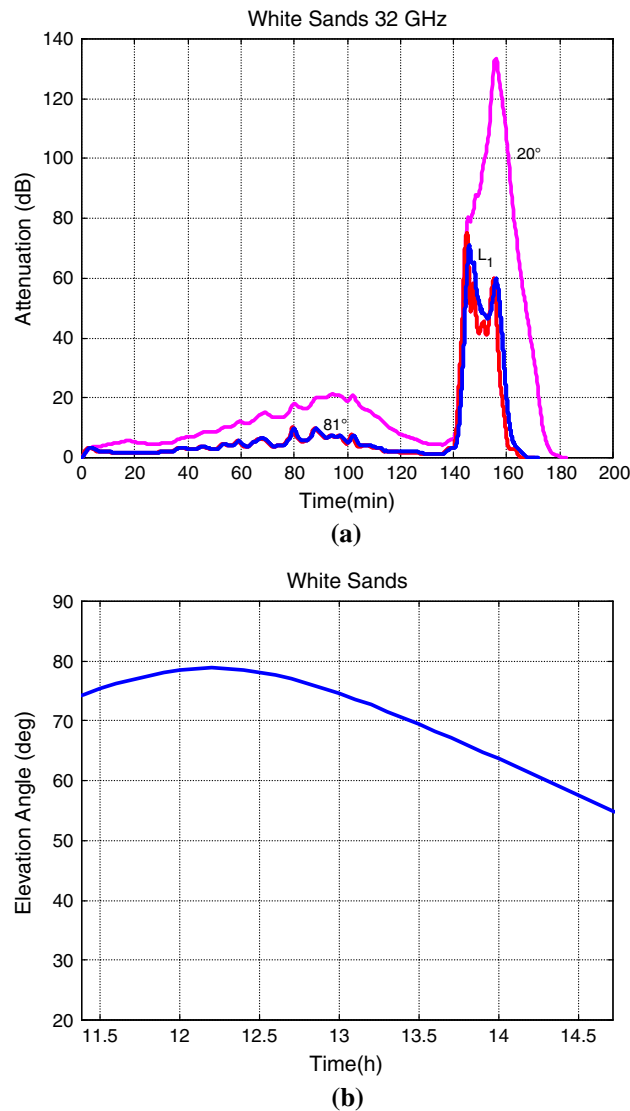


Figure 13. (a) Rain-attenuation time series at 32 GHz, White Sands, July 15<sup>th</sup>, 1996, for the minimum elevation angle to  $L_1$  ( $20^\circ$ , GEO link), magenta line (the high value of the peak attenuation is because of the long path length, that the SST assumes completely filled with rain); maximum elevation angle ( $81^\circ$ , GEO link), red line; for the variable elevation angle to  $L_1$ , blue line; (b) the Sun elevation angle in the same interval of time. Notice that the time axis is the same for both figures (a) and (b), given by the local clock hour  $h_c$ . In (a) time starts at the same hour as in (b), and it is expressed in relative minutes from that instant. In (a), time series have different total durations because of the different elevation angles and rainy path lengths.

appreciable discontinuity is present and so I have been reassured that the 6-min sampling time is effective for the purpose.

It is obvious that the possible contact time with a deep-space probe at  $L_1$  is less in winter than in summer (see Figure 3), and this fact will select particular rain events during the daylight, whose occurrence depends on site climate.

## 5. RAIN ATTENUATION STATISTICAL RESULTS

I report several rain attenuation statistical results with interesting features. Figure 15 shows the rain attenuation pdf at 32 GHz, for White Sands, in three cases: the link to  $L_1$  as described in Section 4 during the contact time, the link to a GEO satellite viewed with an elevation angle  $20^\circ$  (the minimum angle considered to  $L_1$ ), or  $81^\circ$  (the maximum angle found at White Sands in the link to  $L_1$ ) during an average

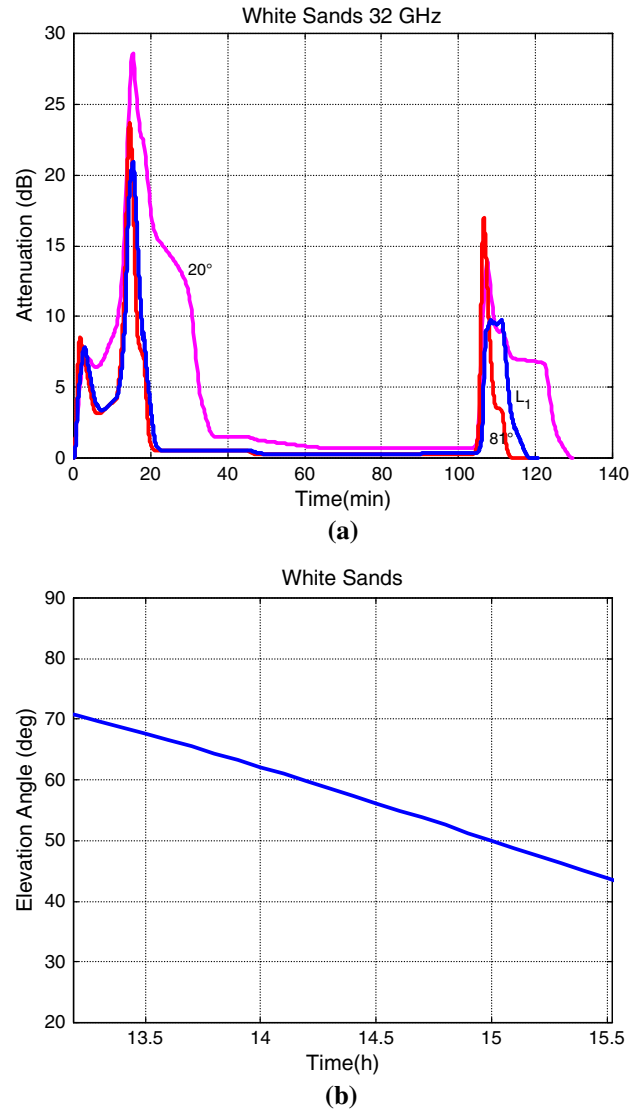


Figure 14. (a) Rain-attenuation time series at 32 GHz, White Sands, July 30<sup>th</sup>, 1997, for the minimum elevation angle to  $L_1$  ( $20^\circ$ , GEO link), magenta line; maximum elevation angle ( $81^\circ$ , GEO link), to  $L_1$ , red line; for the variable elevation angle to  $L_1$ , blue line; (b) the Sun elevation angle in the same interval of time. Notice that the time axis is the same for both figures (a) and (b), given by the local clock hour  $h_c$ . In (a) time starts at the same hour as in (b), and it is expressed in relative minutes from that instant. In (a), time series have different total durations because of the different elevation angles and rainy path lengths.

year. The pdf are normalized to their observation time, therefore to an average year for the GEO paths ( $20^\circ$  and  $81^\circ$ ) because all rain events are observed (24-h observation each day), and to the total time  $\theta_s(t) \geq 20^\circ$  (the contact time with  $L_1$ ), reported in Table III (or Figure 16). We can observe that the  $L_1$  pdf seems to be upper-bounded by the  $81^\circ$  pdf. Notice also that the  $81^\circ$  pdf practically coincides with the  $90^\circ$  pdf (zenith path), which, according to equation (29) of [6], can be calculated directly from the rain-rate pdf (infinite speed case).

Figure 17 shows the results for Tampa at 10 GHz, and Figure 18 shows the results for Spino d'Adda, at 19.7 GHz (the lowest frequency of the current Alphasat Aldo Paraboni Experiment, being now conducted at the site), for  $\theta_s(t) \geq 20^\circ$  in the  $L_1$  link, and in the indicated GEO links. The results of these sites are strikingly different from those found in White Sands, because now the  $L_1$  pdf is in between the minimum elevation-angle GEO pdf and the highest elevation-angle GEO pdf.

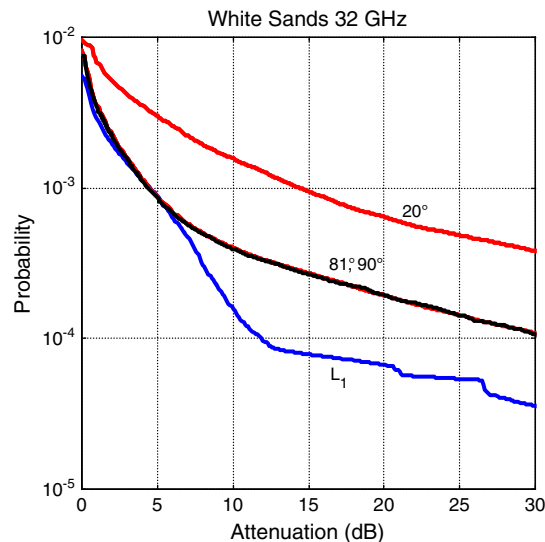


Figure 15. Complementary probability distributions (pdf) (or fraction of the observation time) of rain attenuation at 32 GHz, White Sands, in four links: to  $L_1$  (blue line) as outlined in Section 4, to a GEO satellite viewed with an elevation angle of  $20^\circ$  (the minimum angle considered to  $L_1$  at this frequency, red line), to a GEO satellite with elevation angle  $81^\circ$  (the maximum angle found in the link to  $L_1$ , red line); the superposed black line refers to the zenith link. Except the  $L_1$  pdf, all others are calculated by using all rain events.

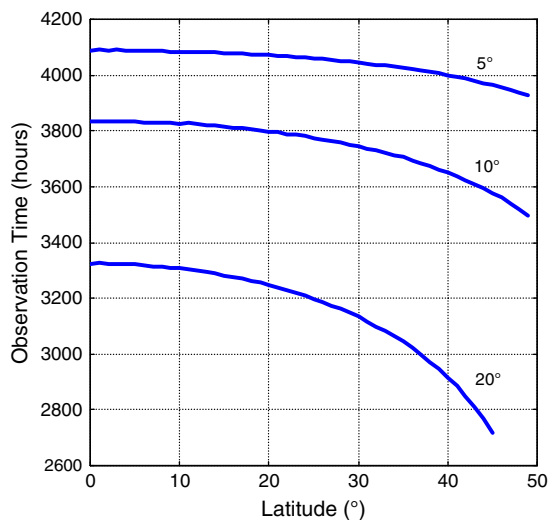


Figure 16. Observation time (h) of the Sun for  $\theta_{\min} = 5^\circ, 10^\circ, 20^\circ$  as a function of latitude.

Let us discuss this behaviour. If the rain events were distributed during the 24 h of a day with no preferred time of occurrence, then the long-term pdf in a slant path with variable elevation angle would be somewhere between the pdf of the minimum and maximum elevation angles in GEO links, probably close to the pdf obtained by assuming the mean elevation angle in the reduced observation (contact) time. In other words, observing the daylight hours with  $\theta_s(t) \geq \theta_{\min}$  would be just like observing the full day. If it is not so, then specific times of occurrence are more probable (e.g. evening, night, early morning, afternoon); therefore the  $L_1$  pdf can be different because it is obtained from a reduced set of rain events with different statistics, compared to the full set. The first case seems to describe the results obtained in Spino d'Adda, for which the  $L_1$  pdf is between the two fixed elevation-angle (GEO) pdf (Figure 18). The second case seems to apply to the other sites, with different grades (Figures 15 and 17).

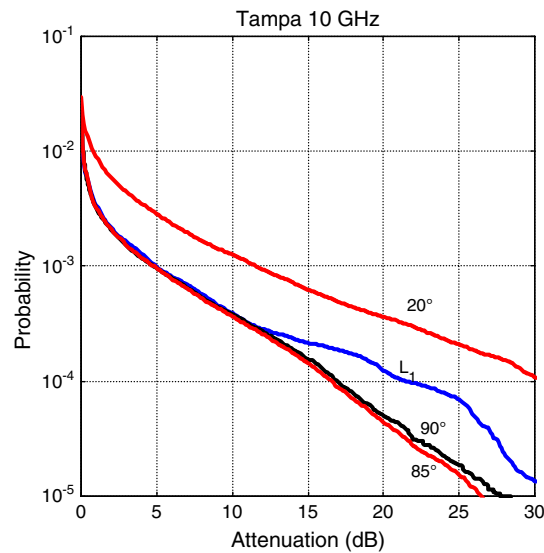


Figure 17. Complementary probability distributions (pdf) (or fraction of the observation time) of rain attenuation at 10 GHz, Tampa, in four links: to  $L_1$  (blue line) as outlined in Section 4, to a GEO satellite viewed with an elevation angle of  $20^\circ$  (the minimum angle considered to  $L_1$  at this frequency, red line), to a GEO satellite with elevation angle  $85^\circ$  (the maximum angle found in the link to  $L_1$ , red line); the superposed black line refers to the zenith link. Except the  $L_1$  pdf, all others are calculated by using all rain events.

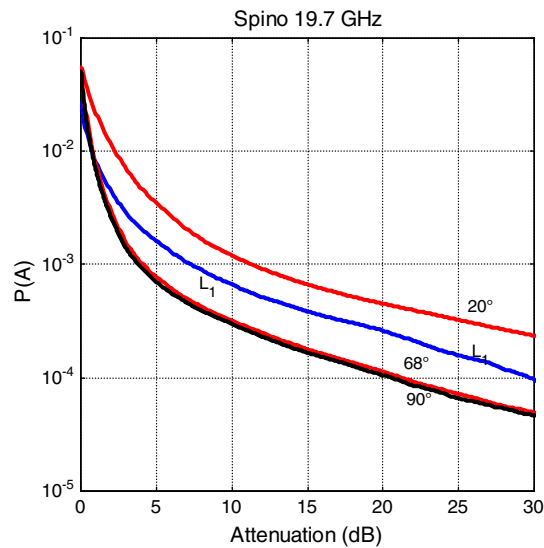


Figure 18. Complementary probability distributions (pdf) (or fraction of the observation time) of rain attenuation at 19.7 GHz, Spino d'Adda, in four links: to  $L_1$  (blue line) as outlined in Section 4, to a GEO satellite viewed with an elevation angle of  $20^\circ$  (the minimum angle considered to  $L_1$  at this frequency, red line), to a GEO satellite with elevation angle  $68^\circ$  (the maximum angle found in the link to  $L_1$ , red line); the superposed black line refers to the zenith link. Except the  $L_1$  pdf, all others are calculated by using all rain events.

Let us discuss more deeply these results. Figures 19–21 show the rain rate pdf exceeded in an average year and in the observation time to  $L_1$  with  $\theta_s(t) \geq 20^\circ$ . As before for rain attenuation pdf, also these pdf are normalized to the observation time, therefore to an average year for the annual pdf, and to the total time  $\theta_s(t) \geq 20^\circ$  for the links to  $L_1$ .

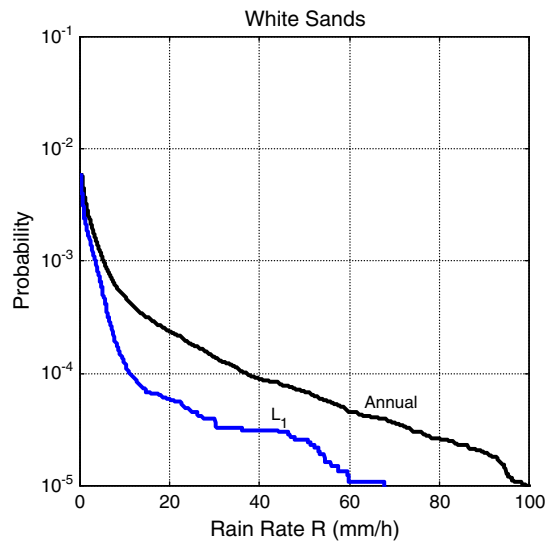


Figure 19. Rain-rate complementary probability (or fraction of the observation time) distributions in an average year (Annual, black), or during the contact time with  $L_1$  (blue line), White Sands.

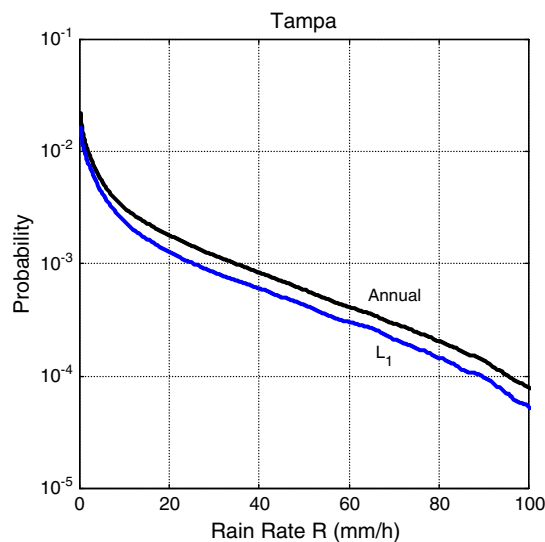


Figure 20. Rain-rate complementary probability (or fraction of the observation time) distributions in an average year (Annual, black), or during the contact time with  $L_1$  (blue line), Tampa.

At White Sands, we can notice that the rain rate pdf is very different from the annual pdf. This means that during the day light, and  $\theta_s(t) \geq 20^\circ$ , a quite statistically different set of rain events is sampled, compared to the full day. Only 52 out of 255 rain events occur (totally or partially) during the observation time (Table III). This number does not change much if we consider the observation time with  $\theta_s(t) \geq 10^\circ$ , passing from 52 to only 71. Table IV reports the total number of rain events per month for each site, for  $\theta_s(t) \geq 20^\circ$  and  $\theta_s(t) \geq 10^\circ$ . Figure 22 shows the scattergram between the two sets to visualize their correlation. We see that: (i) the scattergram concerning White Sands (especially) and Tampa align along the  $y=x$  line, thus meaning that the number of rain events does not change too much by changing the observation time; (ii) the scattergram concerning Spino d'Adda is clearly displaced from the  $y=x$  line, thus meaning that more rain events are included

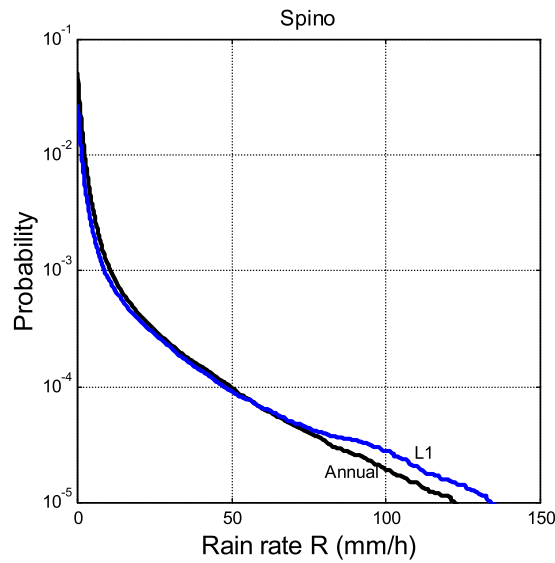


Figure 21. Rain-rate complementary probability (or fraction of the observation time) distributions in an average year (Annual, black), or during the contact time with L<sub>1</sub> (blue line), Spino d'Adda.

Table IV. Total number of rain events per month (1–12), for each site in the L<sub>1</sub> contact time of Table III, according to the minimum elevation angle:  $\theta_s(t) \geq 20^\circ$  (first line),  $\theta_s(t) \geq 10^\circ$  (second line).

Site	1	2	3	4	5	6	7	8	9	10	11	12
Spino d'Adda	13	10	31	52	68	49	37	37	45	27	26	8
	30	17	39	63	75	56	46	48	55	39	45	28
Tampa	10	8	7	14	10	14	18	23	21	9	5	13
	11	9	8	15	14	16	28	32	25	13	5	15
White Sands	2	4	1	2	0	2	9	9	5	7	6	5
	4	6	1	2	0	4	13	10	6	8	9	8

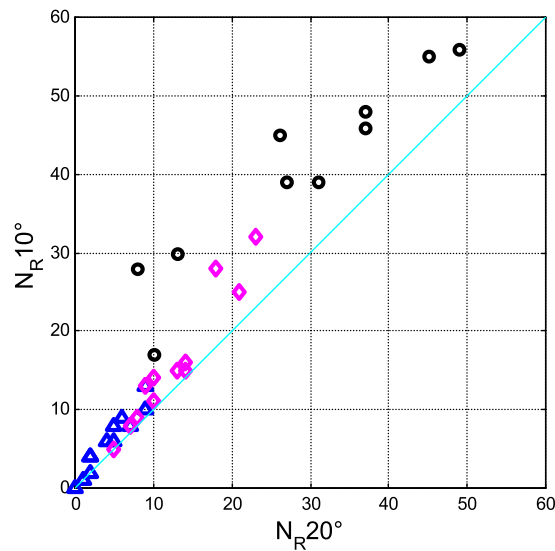


Figure 22. Scattergram between the total number  $N_R$  of rain events considered in the L<sub>1</sub> pdf, for  $\theta_s(t) \geq 20^\circ$  (abscissa) and  $\theta_s(t) \geq 10^\circ$  (ordinate), for each month of the year. Spino d'Adda (black circles); Tampa (magenta diamonds); White Sands (blue triangles).

by increasing the observation time. In other words, the sampling of rain events depends on site and minimum elevation angle; therefore it must affect rain attenuation statistics, as we see next.

Figures 23–25 show the rain attenuation pdf calculated in the link to  $L_1$  by using the SST as described in Section 4, and that calculated: (i) in a slant path with fixed elevation angle (a GEO link) with elevation angle equal either to the mean elevation angle during the contact time with  $\theta_s(t) \geq 20^\circ$  (see (12b)), or equal to the mode (see (11)), with the rain rate pdf of the contact time; (ii) by using the SST in a GEO link with elevation angle equal to the mean elevation angle, as in (i), but with the rain rate pdf of an average year.

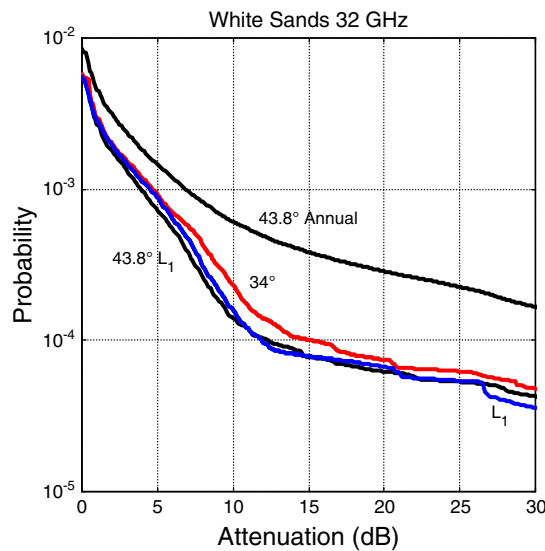


Figure 23. Complementary probability distributions (or fraction of the observation time) at 32 GHz, White Sands: to  $L_1$  (blue line), to a GEO satellite viewed with an elevation angle  $\theta_m = 43.8^\circ$  (lower black line,  $L_1$ ),  $\theta_\mu = 34^\circ$  (red line), by using only the rain events during the contact time, and  $\theta_m = 43.8^\circ$  (upper black line, Annual) by using all rain events.

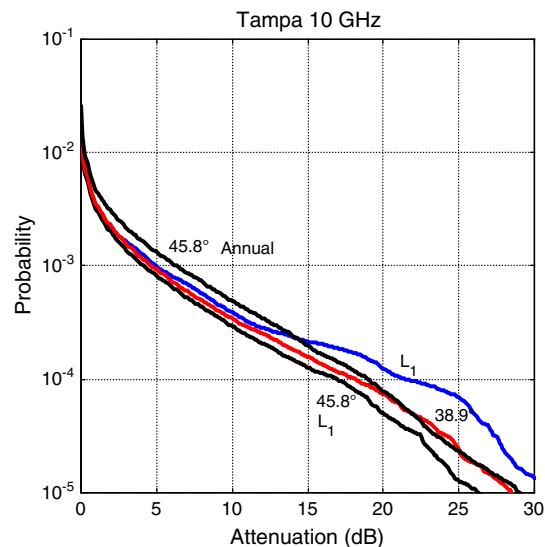


Figure 24. Complementary probability (or fraction of the observation time) distributions at 10 GHz, Tampa: to  $L_1$  (blue line), to a GEO satellite viewed with an elevation angle  $\theta_m = 45.8^\circ$  (lower black line,  $L_1$ ),  $\theta_\mu = 38.9^\circ$  (red line), by using only the rain events during the contact time, and  $\theta_m = 45.8^\circ$  (upper black line, Annual) by using all rain events.

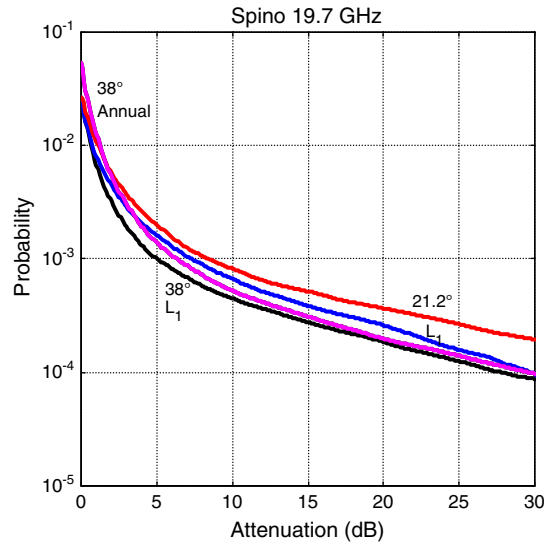


Figure 25. Complementary probability (or fraction of the observation time) distributions at 19.7 GHz, Spino d'Adda: to  $L_1$  (blue line), to a GEO satellite viewed with an elevation angle  $\theta_m = 38.0^\circ$  (lower black line,  $L_1$ ),  $\theta_\mu = 21.2^\circ$ , (red line), by using only the rain events during the contact time, and  $\theta_m = 38.0^\circ$  (magenta line, Annual) by using all rain events.

The comparison between the rain attenuation pdf calculated with the rain rate pdf measured only during the observation (contact) time  $\theta_s(t) \geq 20^\circ$  and that measured with the annual rain rate pdf is straightforward: when the two rain rate pdf are quite different (sampling does affect rain observation), as in White Sands, the two rain attenuation pdf are very different. When the two rain rate pdf are about the same (sampling does not affect rain observation), the two rain attenuation pdf are very alike, as in Tampa and Spino d'Adda, with different grade. Finally, notice that if the mode (11) is assumed in the GEO link, the rain attenuation pdf, at these latitudes (the mode is smaller than the mean with  $\theta_m = 20^\circ$ , see Figure 2), is an upper bound to all predictions.

## 6. CONCLUSIONS

I have investigated how rain attenuation changes in slant paths with variable elevation angles, by simulating rain-attenuation time series with the Synthetic Storm Technique (SST), applied to radio links to a spacecraft located at the Sun–Earth first Lagrangian point  $L_1$ , viewed from three ground sites with different meteorological conditions (Spino d'Adda, Tampa, White Sands, Table I). To a first approximation, the results reported can be also applied to communications with spacecrafts orbiting Mercury, such as the ESA Mercury Planetary Orbiter and the Mercury Magnetospheric Orbiter, both on board the ESA Bepi Colombo spacecraft, because this planet, as seen from the Earth, is angularly close to the Sun.

First, I have summarized known results on the elevation angle of the Sun,  $\theta_s$  ( $^\circ$ ), seen at site at latitude  $\lambda$  ( $^\circ$ ), but I have also found what seems to be a new and interesting result, namely that the most probable value of  $\theta_s$  (the mode of the probability density function of  $\theta_s$  in a year) is given by (11), therefore linked to the Sun–planet orbit. Figure 2 shows all the results concerning  $\theta_s(\lambda)$ , and Table II summarizes the corresponding formulae. These relationships are also valid for the elevation angle of the Sun seen from other planets, for example Mars, by assuming, in this case, the tilt angle  $\varepsilon = 25.19^\circ$ .

Second, I have calculated rain-attenuation time series with the SST. The results show that the complementary probability distribution function (pdf) of rain attenuation in the slant path to  $L_1$ , compared to GEO pdf calculated with several elevation angles at the same site, depends on the rain-rate pdf during the contact time with  $L_1$ , i.e. during the daylight with  $\theta_s(t) > 20^\circ$ . When the

rain rate pdf during the contact time is close to the annual rain rate pdf, then the rain-attenuation pdf during this time is also close to the annual one, and when this condition is not met, the two rain attenuation pdf are different with different grades, depending on the local climate.

To obtain a good estimate of the rain attenuation pdf in the  $L_1$  link without considering a slant path with variable elevation angle, we can consider a GEO link with mean elevation angle (12) and rain rate pdf measured during the contact time, and that the mode (11) gives an upper bound in the sites considered.

In conclusion, the time distribution of the rain events during the 24 h is an important factor when the observation time is only during the daylight, so that the prediction of rain attenuation should consider only the rain rate collected during the expected contact time. The same technique used for the Lagrangian point  $L_1$  could be, of course, developed for LEO, MEO or HEO satellites, once it is suitably adapted to the higher rate of change of the elevation angle, and the shorter intervals of contact time with the ground station. Future work will report this development.

### Appendix A: List of mathematical symbols. Angles are in degrees and depend on latitude (see Table II).

Symbol	Meaning
$\Omega_E$	Peak angle at equinox
$\Omega_{SS}$	Peak angle at summer solstice
$\Omega_{WS}$	Peak angle at winter solstice
$\Omega_{MP}$	Maximum peak angle
$\Omega_{dP}$	Daily peak angle
$\Omega_{dPm}$	Mean daily peak angle
$\Omega_{mP}$	Minimum peak angle
$\alpha$	Constant of specific rain attenuation
$\delta$	Sun declination
$\varepsilon$	Earth-axis tilt angle (obliquity)
$\theta_s$	Sun ( $L_1$ ) elevation angle
$\Delta\theta_s$	Amplitude band of Sun elevation angle $\theta_s$
$\theta_m$	Mean of Sun elevation angle $\theta_s$
$\theta_{\min}$	Minimum elevation angle for contact time
$\theta_\mu$	Mode of Sun elevation angle $\theta_s$
$\lambda$	Latitude
$\tau$	Equation of time (min)
$\phi$	Longitude
$\Omega$	Angle between the meridian plane of the site and of the Sun
$d$	Number of day in a year
$h_c$	Clock (civil) time (h)
$h_s$	Solar time (h)
$k$	Constant of specific rain attenuation
$R$	Rain rate (mm/h)

### Appendix B: The mode

Let us consider a site at latitude  $\lambda$ . Let  $f_k(\theta_s)$  and  $p_k$  be, respectively, the probability density function and statistical weight of the  $k_{th}$  – day of the year, i.e. the duration of the contact time of a day, divided by the total observation time during the contact time in a year. The annual probability density function  $g(\theta_s)$  is given by:

$$g(\theta_s) = f_1(\theta_s)p_1 + f_2(\theta_s)p_2 + \dots + f_{k_{WS}-1}(\theta_s)p_{k_{WS}-1} + f_{k_{WS}}(\theta_s)p_{k_{WS}} + f_{k_{WS}+1}(\theta_s)p_{k_{WS}+1} \dots + f_{365}(\theta_s)p_{365}$$

$$= \sum_{k=1}^{365} f_k(\theta_s)p_k$$

with  $\sum_{k=1}^{365} p_k = 1$  and  $f_{k_{WS}}(\theta_s)p_{k_{WS}}$  refers to the Winter solstice (WS).

Because each density shows a single maximum, taking the derivative of  $g(\theta_s)$ , the mode  $\theta_\mu$  is the solution of the equation:

$$g'(\theta_s) = \sum_{k=1}^{365} f_k'(\theta_s) p_k = 0.$$

A mathematical proof should prove that:

$$f_1'(\theta_\mu) p_1 + f_2'(\theta_\mu) p_2 + \dots + f_{k_{WS}-1}'(\theta_\mu) p_{k_{WS}-1} + f_{k_{WS}}'(\theta_\mu) p_{k_{WS}} + f_{k_{WS}+1}'(\theta_\mu) p_{k_{WS}+1} + \dots + f_{365}'(\theta_\mu) p_{365} = f_{k_{WS}}'(\theta_\mu) p_{k_{WS}} = 0$$

Or, equivalently:

$$f_1'(\theta_\mu) p_1 + f_2'(\theta_\mu) p_2 \dots + f_{k_{WS}-1}'(\theta_\mu) p_{k_{WS}-1} + f_{k_{WS}+1}'(\theta_\mu) p_{k_{WS}+1} + \dots + f_{365}'(\theta_\mu) p_{365} = 0$$

#### ACKNOWLEDGEMENTS

The Author wishes to thank Roberto Acosta, formerly with NASA Glenn Research Center, Cleveland (Ohio), for providing the rain-rate raw data of Tampa and White Sands, and Doriana Giammusso and Nicola Pignatelli, Engineering Telecommunications students at Politecnico di Milano, for developing some basic software tools used in the study.

#### REFERENCES

1. Wilson RW. Sun tracker measurements of rain attenuation at 16 and 30 GHz. *Bell Syst Tech J* 1969; **48**:1383–1404.
2. Davies PG, Lane JA. Statistics of tropospheric attenuation at 190 GHz from observations of solar noise. *Electron Lett* 1970; **6**:522–523.
3. Wrixon GT. Measurements of atmospheric attenuation on an Earth–space path at 90 GHz using a sun tracker. *Bell Syst Tech J* 1971:103–114.
4. Davies PG. Radiometer measurements of atmospheric attenuation at 19 and 37 GHz along Sun–Earth paths. *Proc IEE* 1973; **120**:159–164.
5. Lin SH, Bergmann HJ, Pursley MV. Rain attenuation on Earth–satellite paths—summary of 10 year experiments and studies. *Bell Syst Tech J* 1980; **59**:183–228.
6. Akeyama A, Morita K, Inoue T, Kikushima M, Sasakio, 11- and 18-GHz radio wave attenuation due to precipitation on a slant path. *IEEE Trans Antennas Propag* 1980; **28**:580–585.
7. Davies PG, Mackenzie EC. Review of SHF and EHF slant path propagation measurements made near Slough (UK). *IEE Proc* 1981; **128**:53–65.
8. International Telecommunication Union. Recommendation ITU-R P618-11 Propagation data and prediction methods for the design of Earth–space telecommunication systems, 2013, P Series Radiowave Propagation.
9. Roselló J, Martellucci A, Acosta R, Nessel J, Bråten LE, Riva C. 26-GHz data downlink for LEO satellites, *6th European Conference on Antennas & Propagation*, EuCAP 2012, 111–115, 26–30 March 2012, Prague.
10. Liu W, Michelson D. Fade slope analysis of Ka-band Earth–LEO satellite links using a synthetic rain field model. *IEEE Trans Veh Technol* 2009; **58**:4013–4022.
11. Kourogorgas CI, Panagopoulos AD. A rain attenuation stochastic dynamic model for LEO satellite systems above 10 GHz. *IEEE Trans Veh Technol* 2015; **64**:829–834.
12. Matricciani E. Physical–mathematical model of the dynamics of rain attenuation based on rain rate time series and two layer vertical structure of precipitation. *Radio Sci* 1996; **31**:281–295.
13. Meeus J. *Astronomical Algorithms*. Willmann-Bell, Richmond: Virginia, 1991.
14. Cooper PI. The absorption of radiation in solar stills. *Solar Energy* 1969; **12**:333–346.
15. ITU-R Rain height model for prediction methods, ITU-R P series recommendations—radiowave propagation. Long-term Ka/Ku-band slant path rain attenuation and rain rate statistics. P.839–3, 2001, Geneva.
16. Matricciani E. Rain attenuation predicted with a two-layer rain model. *Eur Transac Telecommun* 1991; **2**:715–727.
17. Maggiori M. Computed transmission through rain in the 1–400 GHz frequency range for spherical and elliptical drops and any polarization. *Alta Frequenza* 1981; **50**:262–273.

## AUTHOR'S BIOGRAPHY



**Emilio Matricciani** was born in Italy, in 1952. After serving in the Italian Army, he received the Laurea degree in Electronics Engineering at Politecnico di Milano, Milan, Italy, in 1978. He joined Politecnico di Milano in 1978 with a research scholarship, and in 1981 he became assistant professor of Electrical Communications. In 1987, he joined Università di Padova, Padua, Italy, as associate professor of Microwaves. In 2001, he qualified as full professor of Telecommunications. Since 1991, he has been working with Politecnico di Milano, as professor of Telecommunications. His research interests include satellite communications for fixed and mobile systems, deep-space communications, radio propagation at millimetre waves, rain effects on satellite system design and history of science. Most of his early experimental and theoretical activities concerned the propagation and communication experiments devised at Politecnico di Milano by Francesco Carassa and Aldo Paraboni (satellites SIRIO, ITALSAT and ALPHASAT Aldo Paraboni experiment). In the '90s and in the 2000s, he has conducted extensive research on communications with mobile terminals running in the rain and linked to satellites in the geostationary orbits, or in lower orbits, and on developing rain attenuation prediction models useful to predict first order (probability distribution functions) and second order (fade durations, rates of change and unavailability during the time of the day) statistics for satellite systems design, such as the Synthetic Storm Technique. In addition to the institutional activities, such as lectures on Terrestrial and Satellites Radio Relays, he teaches Scientific Writing to PhD students at Politecnico di Milano and in other Italian Universities.